IEEE Access
Multidisciplinary | Rapid Review | Open Access Journal

Received February 8, 2021, accepted February 25, 2021, date of publication March 1, 2021, date of current version March 12, 2021.

Digital Object Identifier 10.1109/ACCESS.2021.3062829

An Electronic Line-Shafting Control Strategy Based on Sliding Mode Observer for Distributed Driving Electric Vehicles

HAO HUANG, QUNZHANG TU, CHENGMING JIANG, MING PAN, AND CHANGLIN ZHU
Field Engineering College, Army Engineering University of PLA, Nanjing 210007, China

Corresponding author: Qunzhang Tu (tqzlhnj@126.com)

This work was supported in part by the National Key Research and Development Plan of China under Grant 2016YFC0802903, and in part by the National Natural Science Foundation of China under Grant 61671470.

ABSTRACT This paper proposed control schemes to realize the collaborative control as well as enhance the control precision for the distributed driving electric vehicle (DDEV). Firstly, we suggested an electronic line-shafting (ELS) to realize the cooperative control for the Multi-Motor system which is installed in the DDEV. Secondly, we adopted a nonsingular terminal sliding mode control (NTSMC) method combined with a sliding mode observer (SMO) to quicken the response velocity and strengthen the robustness of the single motor controller. Finally, for the chattering value caused by the internal parameter variation and external disturbance, a fuzzy algorithm is proposed to obtain the controller parameters of NTSMC in real-time to eliminate the chattering value of DDEV. Through several simulations and experiments, the results demonstrate that the proposed strategies can realize ideal collaborative control for the Multi-Motor system, as well as improve the dynamic performance and anti-jamming ability for the whole control system of DDEV.

INDEX TERMS Distributed driving electric vehicle, multi-motor system, electronic line-shafting, nonsingular terminal sliding mode control, sliding mode observer.

I. INTRODUCTION

In the last decades, the vehicle transportation system is occupying a huge proportion of human life, while the traditional vehicle industry can conduct to severe environmental pollution and energy consumption, which leads to the increasing demand for energy-saving and environment -friendly automobile such as electric vehicle (EV) [1]. Due to the breakthrough of the key technology of the electric motor and motor controller, the EV industry is becoming a research hotspot recently, which possesses the merits of high driving safety and transmission efficiency [2], [3]. Nowadays, there are two main types of transmission structures for EV, namely centralized drive and distributed drive [4]. The transmission structure of the centralized drive is very similar to the traditional engine structure, and this structure uses the electric motor to replace the vehicle engine as the energy device, but there is no change in other transmission devices. The centralized drive has the merit of the simple control structure and stable control process, but it cannot improve the transmission efficiency and control precision of EV due to its transmission structure [5]. The distributed drive is an advanced form of EV, the main characteristic of which is electric motors are installed in the wheel of EV. The transmission structure of distributed drive can remove some mechanical transmission parts such as gearbox, differential, and transmission shaft, so this transmission type has the advantages of high space utilization, compact structure, and precise control due to its shorter control chain [6], [7]. Therefore, the distributed driving electric vehicle (DDEV) provides a brilliant prospect for the vehicle industry.

Although DDEV has the above merits during the driving period, there are three key problems that need to be solved during the driving period of the DDEV. Firstly, because DDEV eliminates differential in the automobile, when the automobile crosses a rough road or turn, the torque received by the in-wheel motor will be variable, which can conduct to the speed of motor deviate from the command value [8]. Secondly, the mechanical parameters of in-wheel motors installed in the wheel can change due to the frequent

The associate editor coordinating the review of this manuscript and approving it for publication was Nasim Ullah.

vibration, temperature change, and parts aging, which may lead to the response time and the output speed are different between motors when receiving the same command [9]. Thirdly, the control strategy of the motor can also affect the driving efficiency of DDEV speed, if the control strategy is not optimal enough and cannot achieve the response in the given time, the vehicle will be unstable and unsafe. These issues above can lead to the imbalance and control error of the in-wheel motor installed in the DDEV, and may further lead to skidding, idling, and rollover of DDEV [10].

In order to solve the issues presented above, Zhang *et al.* proposed an algorithm based on a novel fuzzy observer-based steering control which aiming at solving path tracking control for distributed control object [11]. Zhao *et al.* established the simulation model of DDEV and adopted a slip rate control scheme to realize the synchronous coordinated control [12]. Wang *et al.* built a dynamic EV model and suggested the hierarchical coordination control approach for coordination control [13]. Park *et al.* built the EV mathematical model and simulate the special conditions for the driving and steering of the vehicle [14]. Huang *et al.* proposed a fast terminal sliding mode algorithm for control of the in-wheel motor of DDEV, this control scheme is not sensitive to the change of internal parameters of the motor and can effectively improve the control precision of the single motor [15]. Zhang adopted a sliding-mode observer to adjust the parameters variation and efficiently reduce the disturbances caused by the internal parameter fluctuation of motor [16], [17] presented a nonlinear optimal finite-time tracking controller based on a state-dependent Riccati equation for the Multi-Motor driving system, which adopted nonlinear sliding mode controller to overcome the approaching problem of conventional SMC. Reference [18] presented a novel nonlinear decoupling control scheme based on radial basis function neural network inverse for permanent magnet in-wheel motors (PMIWM), and this method improved the anti-jamming performance and control precision of the controller.

These methods proposed above can effectively enhance the control efficiency and control precision of DDEV, while there are two issue that still need to be solved. Firstly, former research cannot realize the cooperative control when this vehicle undergoes variable external disturbance, which can conduct to the inconsistent speed of each motor. In addition, the response speed and robustness of the single PMIWM installed in the DDEV should be further optimized to improve the performance of this type of vehicle in order to improve the safety and comfort of it.

With the motivation of solve the problems that not be studied by the former researcher and optimizing the driving safety and control efficiency of DDEV, we proposed a novel electronic line-shafting (ELS) to achieve the cooperative control of each motor installed in the DDEV, and the total-amount coordinated control (TACC) applied in this algorithm can adjust the speed of each motor in real-time. Also, aimed at the problems that internal parameters of each in-wheel motor cannot be a constant when the DDEV is driving, we applied a nonsingular terminal sliding mode control (NTSMC) to eliminate the influence of the parameters and improve the anti-jamming performance of the single-motor controller. For the propose of further optimizing the NTSMC and reduce the chattering value of DDEV, we adopted a fuzzy algorithm to observe the control parameters of NTSMC and enhance the precision of the motor, as well as adopted a load torque observer based on sliding mode observer (SMO) to compensate the external load torque in real-time. We denote the proposed method for the Multi-Motor system as ELS strategy and the method for the single motor as SMO-NTSMC strategy. The major contributions of this paper are as follows:

1) A novel ELS control method on the basis of the TACC algorithm is suggested to realize the synchronous control of each in-wheel motor installed on the DDEV. This scheme can effectively optimize the control accuracy and anti-interference ability of the total motor control system.
2) For the purpose of improving the response performance and eliminating the influence of parameters for a single in-wheel motor, we applied an NTSMC to realize that the control error can be eliminated within finite time.
3) Aiming at solving the problem of the chattering value arises during the period of NTSMC, we suggested a fuzzy algorithm to observe the control parameters in real-time, which can effectively overcome the chattering phenomenon and enhance the anti-jamming ability of the control system.

The paper is organized as follows. In Section 2, the mathematical models of DDEV and in-wheel motor are designed. In Section 3, the ELS control algorithm based on the TACC algorithm is suggested to achieve the synchronous control of the total motor control system. In Section 4, we applied an NTSMC strategy to improve the control accuracy of the single motor, as well as designed fuzzy rules to search the ideal control parameters for NTSMC, as well as adopted a load torque observer to compensate for the external torque. Numeral co-simulation and physical experiments are implemented, and the results are discussed in Section 5. Section 6 summarizes the whole paper.

II. SYSTEM MODELING

In this section, a DDEV control model is established through using Carsim and Simulink software, and a simplified PMIWM model is built through Matlab/Simulink, the motion equation of DDEV and PWIWM will be designed to determine the accurate mathematical model.

A. MATHEMATICAL MODEL OF DDEV

The configuration of DDEV driven by 4 PMIWM is shown in Fig 1, in this chassis layout of DDEV, the vehicle controller sends control signals to 4 in-wheel motor controllers respectively and receives torque and speed information from 4 controllers to adjust control signals in real-time. Each PMIWM of the DDEV control system is driven through the controller to

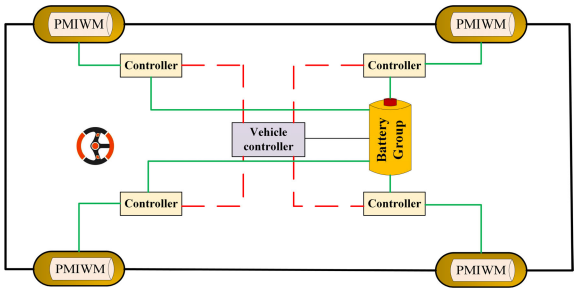

FIGURE 1. Chassis layout of DDEV driven by 4 PMIWM.

produce traction torque and provides the driving force for the corresponding wheel. In this paper, driving and steering of the DDEV are controlled by two front in-wheel motors [19], [20].

Consider the dynamic model of DDEV, state of the vehicle is defined by the second Newtons' law, and the longitudinal equation of motion is expressed as [21]

$$ma_x = m(\dot{v}_x - v_y\omega_z + v_z\omega_y) \tag{1}$$

Lateral longitudinal motion equation is written as

$$ma_y = m(\dot{v}_y - v_z\omega_x + v_x\omega_z) \tag{2}$$

Vertical motion equation is written as

$$m_s(v_z - v_x\omega_y - v_y\omega_x) = F_{z\_f}l + F_{z\_f}r + F_{z\_rl} + F_{z\_rr} - mg \tag{3}$$

Rolling equation of motion is written as

$$I_x a_x - (I_y - I_z)\omega_y\omega_z = -\frac{B_f}{2}(F_{z\_fl} + F_{z\_fr}) + \frac{B_r}{2}(F_{z\_fl} + F_{z\_rr}) \tag{4}$$

Pitch motion equation is written as

$$I_y a_y - (I_z - I_x)\omega_z\omega_x = -\frac{l_f}{2}(F_{z\_fl} + F_{z\_fr}) + \frac{l_r}{2}(F_{z\_fl} + F_{z\_rr}) \tag{5}$$

where m is the vehicle weight. m_s is the sprung mass, g is the acceleration of gravity. v_x, v_y and v_z are the vehicle speed on x-axis, y-axis and, z-axis, respectively. ω_x, ω_y and ω_z are the angular velocity of the vehicle on x-axis, y-axis, and z-axis, respectively. a_x and a_y are the longitudinal acceleration and the lateral acceleration of the vehicle, respectively. B_f and B_r are the wheelbase of the front and rear wheels. l_f and l_r are the distance from the front axle and rear axle to the center of the mass. F_{z_fl}, F_{z_fr}, F_{z_rl}, and F_{z_rr} are the longitudinal force of the left of the front axle, the right of the front axle, the left of the rear axle, and the right of the rear axle, respectively. I_x, I_y and I_z are the moment inertia of the vehicle on x-axis, y-axis, and z-axis, respectively.

The wheel slip ratio λ is defined as [22]

$$\begin{cases} \lambda = \dfrac{r_t\omega - V}{r_t\omega} & \text{for driving} \\ \lambda = \dfrac{V - r_t\omega}{r_t\omega} & \text{for braking} \end{cases} \tag{6}$$

where r_t is the wheel radius, and V is the vehicle speed. According to [23], [24], friction coefficient shows similar characteristics for various road conditions, which increases with increasing λ up to some point and then decreases. Even if there is a difference in absolute value, we note that the maximum friction coefficient exists in the range of $\lambda = 0.15 \sim 0.2$ for each road condition. Therefore, in this study, the slip ratio is controlled in the range $\lambda = 0.15 \sim 0.2$.

B. MATHEMATICAL MODEL OF PMIWM

In order to simplify the mathematical model of PMIWM, surface-mounted installation mode is adopted for permanent magnets in motors, and the control current for the PMIWM system can be expressed as follows:

$$\begin{cases} \dfrac{di_d}{dt} = -\dfrac{R}{L_d}i_d + \dfrac{L_q}{L_d}\omega i_q + \dfrac{u_d}{L_d}u_d \\ \dfrac{di_q}{dt} = -\dfrac{R}{L_q}i_q - \dfrac{L_q}{L_d}\omega i_d + \dfrac{1}{L}u_q - \dfrac{1}{L}\psi_f \end{cases} \tag{7}$$

where i_d and i_q are the current of $d-q$ axis respectively, L is the self-inductance, L_d and L_q are the inductance of $d-q$ axis respectively, R is the stator resistance, u_d and u_q are the voltage of $d-q$ axis respectively, ψ_f is permanent magnet flux linkage of the motor, ω is the rotating angular velocity of PWIWM, and the dynamic equation of PWIWM is expressed as follows:

$$\begin{cases} T_e - T_L = J\dfrac{d\omega}{dt} \\ T_e = \dfrac{3}{2}P\left[\left(L_d - L_q\right)i_d i_q + \psi i_q\right] \end{cases} \tag{8}$$

Based on the surface-mounted installation of PMIWM, $L_d = L_q = L$, Equation (8) can be simplified as follows:

$$\ddot{\theta} = \frac{3}{2J}P\psi i_q - \frac{T_L}{J} \tag{9}$$

The control system layout of PMIWM established based on Matlab/Simulink is presented in Fig 2. field-Oriented control (FOC) structure and $i_d = 0$ is adopted in this control diagram, motor speed ω and current of i_q are two closed-loop in this control process to eliminate control error [25].

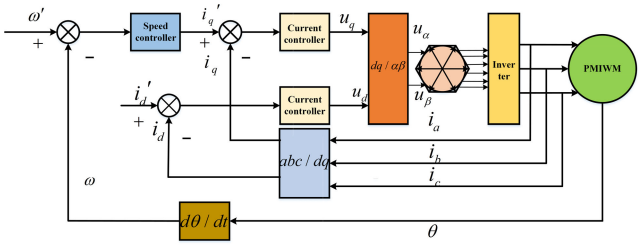

FIGURE 2. Control diagram of the PMIWM system.

III. CONTROLLER DESIGN

The proposed strategy in this paper can be divided into three parts. Firstly, aiming at realizing the synchronous control of two drive in-wheel motor which installed in the front

wheel, we propose an ELS control strategy combined with a load torque observer. Secondly, an NTSMC algorithm is suggested to improve the controller precision and robustness of each in-wheel motor. Thirdly, we adopt a fuzzy algorithm to eliminate the chattering value, as well as adopt a sliding mode observer to compensate for the fluctuation of external load torque.

A. ELS CONTROLLER DESIGN

In this ELS controller, we denote a virtual electronic shaft as a master physical shaft, which can control and drive the other slave in-wheel motor through the control signal. As shown in Fig 3, the target of this control algorithm is to make the speed error between the Multi-motor system and the virtual motor and ELS controller converge to zero. When the motor is disturbed, the output speed of each in-wheel motor is different from each other, the ELS receives the feedback from the output speed signal for each motor and adjust the total speed control signal until the motor control system reaches the steady-state [26].

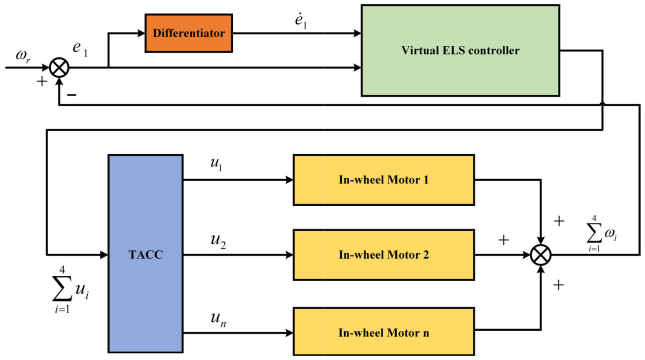

FIGURE 3. TACC method for controlling distributed system.

Because this distributed-motor system demands high-precision and suitable control parameters, a total sliding mode algorithm is suggested for this controller, which has the merits of high control efficiency, strong robustness, and precision tracking control [27]. In order to realize that the total speed of the distributed-motor l system can track the given speed of the virtual ELS, we denote the error of them as e_1, and the tracking error of the distributed-motor can be expressed as following [28], [29]:

$$e_1 = \sum_{i=1}^{4} \omega_i - \omega_r = \sum_{i=1}^{4} x_{i1} \tag{10}$$

Take the derivative of Equation (10)

$$\dot{e}_1 = \sum_{i=1}^{4} \dot{\omega}_i - \dot{\omega}_r = \sum_{i=1}^{4} x_{i2} \tag{11}$$

Select the surface as follows:

$$s_1 = ce_1 + \dot{e}_1 \tag{12}$$

Simplified the motor equation (9) and the following dynamic model can be obtained:

$$J\ddot{\theta}_i = u_i + d_i(t) \tag{13}$$

where $u_i = \frac{3}{2}P\psi iqi$, and denote u as the TACC protocol, $d_i(t) = TLi$.

Design the TACC protocol as

$$u_i = -\eta_i \operatorname{sgn}(s_1) - d_i(t) - Jc\omega_i + \frac{1}{4}(\omega_r + \dot{\omega}_r) \tag{14}$$

where approaching parameter $c > 0$, $\operatorname{sgn}(s_1)$ is sign function.

Select the Lyapunov function as follows:

$$V_1 = \frac{1}{2}s_1^2 \tag{15}$$

According to the above Equations, the differentiation of V_1 can be obtained as:

$$\begin{aligned} \dot{V}_1 &= \dot{s}_1 s_1 = s_1(-cs_1 - \frac{1}{J}\eta \operatorname{sgn}(s_1) + \frac{1}{J}d(t)) \\ &= \frac{1}{J}(-cs_1^2 - \eta |s_1| + s_1 d(t)) \le -\frac{1}{J}cs_1^2 \end{aligned} \tag{16}$$

Because J and c are positive odd numbers, $\dot{V}_1 \le 0$, It can be seen from Equation (16), this control system is stable.

B. DESIGN OF SPEED AND CURRENT CONTROLLER

In the conventional SMC strategy, a linear sliding mode surface is frequently adopted to eliminate control error. However, this sliding mode surface cannot converge to zero in a limited time, which is not suitable for high precision control of a single motor [30]. Aiming at solving this problem, [31] adopted a terminal sliding mode surface to substitute for the conventional linear sliding mode surface. Terminal sliding mode surface owns the characteristic that can converge to zero in a limited time, but it is possible to occur the singular phenomenon in the control process, so we design a nonsingular terminal sliding mode surface to realize ideal control performance of the single in-wheel of DDEV system.

The NTSMC proposed to optimize the single motor system owns two merits. Firstly, the sliding mode surface adopted in this controller can converge to zero in finite time and can obtain quicker response speed than the conventional SMC. Secondly, this nonsingular terminal sliding mode surface can overcome the nonlinear singularity phenomenon during the control process. The control effect of the NTSMC is presented in detail in Section IV.

The state parameters are denoted as following in the NTSMC strategy:

$$\begin{cases} x_1 = \omega_i' - \omega_i \\ x_2 = \dot{x}_1 = \dot{\omega'}_i - \dot{\omega}_i \end{cases} \tag{17}$$

where x_1, x_2 are state parameters of speed, ω' is the command speed, and ω is the output speed.

Denote the nonsingular terminal sliding mode surface as following [32]:

$$s_2 = x_1 + \frac{1}{\beta}x_2^{p/q} \tag{18}$$

where β, p and q are control parameter of NTSMC, $\beta > 0$, p and q are positive odd number and $p > q$.

Denote the single in-wheel motor as a second-order dynamic system

$$\begin{cases} \dot{x}_1 = x_2 \\ \dot{x}_2 = f(x) + gu + d(t) \end{cases} \tag{19}$$

According to (10), $f(x) = 0$, $g = \frac{1}{J}$, $d(t) = T_L$. Design the NTSMC protocol as

$$u = -g^{-1}(x)(f(x) + \beta \frac{q}{p} x_2^{2-p/q} + (D + \eta)\text{sgn}(s_2)) \tag{20}$$

where $1 < p/q < 2$, $\eta > 0$, $|d(t)| \leq D$, and $d(0) = 0$, because $d(t)$ is time-variant, the value of can be obtained through the adaptive method applied in the [33], [34]

Select the Lyapunov function to verify the stability of this NTSMC system:

$$\begin{aligned} \dot{V}_2 &= s_2 \dot{s}_2 = s_2 \cdot (\dot{x}_1 + \frac{1}{\beta}\frac{p}{q} x_2^{p/q-1} \dot{x}_2) \\ &= s_2 \cdot \left(x_2 + \frac{1}{\beta}\frac{p}{q} x_2^{p/q-1} (f(x) + g(x)u + d(t)) \right) \\ &= s_2 \cdot \left(\frac{1}{\beta}\frac{p}{q} x_2^{p/q-1} (-(D + \eta)\text{sgn}(s_2) + d(t)) \right) \\ &= \frac{1}{\beta}\frac{p}{q} x_2^{p/q-1} (s_2 d(t) - (D + \eta)\,|s_2|) \end{aligned} \tag{21}$$

Because $1 < p/q < 2$, and $\beta > 0$, then

$$s_2 \dot{s}_2 \leq \frac{1}{\beta}\frac{p}{q} x_2^{p/q-1} (-\eta\,|s|) \tag{22}$$

It is obvious that when $x_2 \neq 0$, the controller satisfies the stability conditions for the Lyapunov equation.

Because the current loop of the whole control system plays less important role in the control precision than the speed loop, in order to lessen the computational burden, we proposed a simpler SMC for this loop and analyze the stability of it.

$$\begin{cases} x_3 = iq_i' - iq_i \\ x_4 = \dot{x}_3 = \dot{iq}_i' - \dot{iq}_i \end{cases} \tag{23}$$

where x_3, x_4 are state parameters of current i_q, $i_{q'i}$ and i_{qi} are the output current and input current, respectively.

Select the sliding mode surface of i_q as follows:

$$s_3 = x_3 \tag{24}$$

Denote the reaching law of the sliding mode surface as:

$$\dot{s}_3 = -k\ \text{sgn}(s_3) \tag{25}$$

It is obvious that $s_3 \dot{s}_3 \leq 0$, according to Lyapunov function, we can prove the stability of the current loop.

According to (7), the control input u_{qi} can be obtained as follows:

$$u_{qi} = L\frac{di_{q'i}}{dt} + Ri_{qi} + \omega\psi_f - k\ \text{sgn}(s_3) \tag{26}$$

Similarly, select the same surface s_4 for the current i_d and the stability can be proved as i_q, and the control input u_{di} can be expressed as follows:

$$u_{di} = L\frac{di_{d'i}}{dt} + Ri_{di} - \omega L i_q - k\ \text{sgn}(s_4) \tag{27}$$

C. DESIGN OF FUZZY CONTROLLER AND SMO

Because PMIWM installed in the DDEV is sensitive to parameters variation and external influence, which can cause a chattering phenomenon that can weaken the robustness and control accuracy of the DDEV [35]. Besides, if the chattering phenomenon is in excessive inhibition, the robustness of the control object will be weakened, which will deteriorate the anti-jamming ability of the PMIWM system. Therefore, how to make a balance of overcoming the chattering value as well as realizing optimal robustness of the control object is a key issue that needs to be solved.

In order to overcome the above issues and further optimize the dynamic performance of the in-wheel system. Firstly, we designed fuzzy rules in this section to adjust the control parameter η of the NTSMC in real-time to eliminate the interference of the chattering value as well as optimize the anti-jamming ability of the control system. Secondly, a load torque observer is proposed to detect and feedback the external disturbances of the in-wheel motor. This method can effectively weaken the influence of external disturbance.

Because η is designed as the control parameter for the NTSMC strategy, and η is the key factor to affect the approaching speed and chattering value during the control process [36], [37]. Aiming to decrease the chattering phenomenon as well as realize ideal anti-interference capability, a fuzzy algorithm is suggested to obtain η sgn(s) online.

Denote the output of the fuzzy system as

$$\hat{h}(s\,|\theta_h^*) = \eta\ \text{sgn}(s) \tag{28}$$

where θ_h^* is the optimal parameter and denote the adaptive law $\hat{\theta}_h$ as follows:

$$\hat{\theta}_h = \gamma s \phi(s) \tag{29}$$

where γ is adaptive control parameter and $\gamma > 0$.

Denote the optimal parameter θ_h^* as

$$\theta_h^* = \arg \min_{\hat{\theta}_h \in \Omega_h} [\sup \left| \hat{h}(s\,|\hat{\theta}_h) - \eta\ \text{sgn}(s) \right|] \tag{30}$$

where Ω_h is the set of $\hat{\theta}_h$

In the fuzzy controller designed in this section for the in-wheel control system, s and $\phi(s)$ are denoted as fuzzy inputs and $\hat{h}(s\,|\theta_h^*)$ is denoted as fuzzy output, the corresponding relation of input and output is designed as Table 1, and the degree of membership for the fuzzy parameters is shown in Fig 4.

Through adopting the fuzzy controller, the approaching parameter in the NTSMC strategy $\hat{h}(s\,|\theta_h^*)$ can be obtained online for the PMIWM system. Using $\hat{h}(s\,|\theta_h^*)$ to replace the

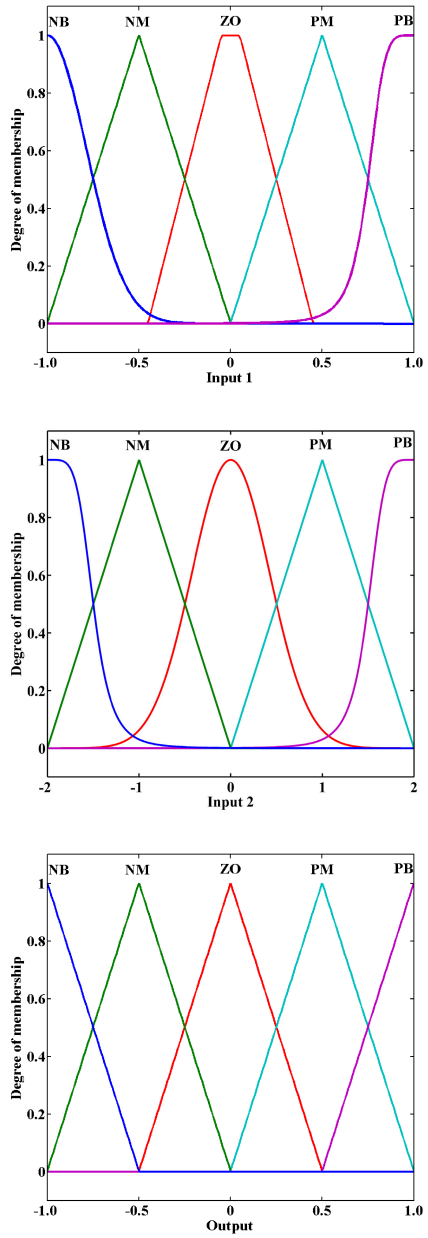

FIGURE 4. The degree of membership for the fuzzy parameters (a) Input s (b) Input $\phi(s)$ (c) Output $\hat{h}(s\left|\theta_h^*\right.)$.

$\eta\ \mathrm{sgn}(s)$ in Equation (14) and the full expression of NTSMC can be obtained as follows:

$$u_2 = -g^{-1}(x)(f(x) + \beta\frac{q}{p}x_2^{2-p/q} + \hat{h}(s\left|\theta_h^*\right.) + d(t)\mathrm{sgn}(s)) \tag{31}$$

Because there are lots of parameter variation during the driving period of the DDEV, especially the external load torque T_L, the variation of this value can lead to undesirable control accuracy, limit cycles, and even instability. In order to compensate the external load torque of the control system in real-time, an estimation scheme on the basis of SMO is developed with the inspiration of [38].

The SMO algorithm owns the merits such as simple implementation, precision estimation ability, and strong robustness [39]. In this method, we assumed that the load torque of the control system is a constant for a short period, and Equation (9) can be expressed as follows [40]:

$$\begin{cases} \dfrac{d\omega}{dt} = \dfrac{T_e}{J} - \dfrac{T_L}{J} \\ \dot{T}_L = 0 \end{cases} \tag{32}$$

In this load torque observer, we denote the output angular acceleration and load torque objects for the SMO, and an extended sliding mode observer is designed as follows:

$$\begin{cases} \dfrac{d\hat{\omega}}{dt} = \dfrac{\hat{T}_e}{\hat{J}} - \dfrac{\hat{T}_L}{\hat{J}} - ks_m \\ \dot{\hat{T}}_L = gs_m \end{cases} \tag{33}$$

where $\hat{\omega}$, $\hat{T}_e$, $\hat{T}_L$ and $\hat{J}$ are the observe values of ω, T_e, T_L and J respectively. k and g are the sliding mode gain and the feedback gain, respectively. $s_m = \mathrm{sgn}(\omega_r - \omega)$.

Denote $e_3 = \hat{\omega} - \omega$ and $e_4 = \hat{T}_L - T_L$, combine (32) with (33) and the state equation of SMO can be obtained as follows:

$$\begin{cases} e_3 = M - ks_m \\ e_4 = gs_m \end{cases} \tag{34}$$

where

$$M = \frac{\hat{T}_e - \hat{T}_L}{\hat{J}} - \frac{T_e - T_L}{J} \tag{35}$$

Define the sliding surface as follows:

$$s_3 = e_3 = \omega_r - \omega \tag{36}$$

Based on the Lyapunov function, the stable condition of the SMO is $s_3\dot{s}_3 \le 0$, according to (36) and (34), we have

$$s_3\dot{s}_3 = e_3\dot{e}_3 = e_3(M - ks_m) \tag{37}$$

When equation (37) satisfies the stable condition of the Lyapunov function, the parameter k can be obtained as follows:

$$k \ge |M| \tag{38}$$

When the sliding mode observer approaches the sliding mode, $e_3 = \dot{e}_3 = 0$ is satisfied. Then Equation (34) can be simplified as:

$$\begin{cases} M - ks_m = 0 \\ \dot{e}_4 = gs_m \end{cases} \tag{39}$$

From (39), the state equation of the SMO is derived as:

$$\dot{e}_4 - \frac{gM}{k} = 0 \tag{40}$$

Combine (40) with (35), and the following equation can be obtained:

$$\dot{e}_4 - \frac{g}{k\hat{J}}e_4 - \frac{g(T_e - T_L)}{kJ} = 0 \tag{41}$$

Solution (41) and the observer error can be obtained as follows:

$$e_4 = Ce^{\frac{g}{kJ}t} - \frac{(T_e - T_L)\hat{J}}{J} \tag{42}$$

On the basis of the above algorithm, we can compensate for the error of the external disturbance in real-time, which can eliminate the influence of the external disturbance and strengthen the robustness of the controller.

IV. SIMULATION AND EXPERIMENTS

In this section, we implemented several simulations and experiments on the in-wheel motor system and discussed some experimental results in detail. The results verify the availability and effectiveness of the control methods

A. IMPLEMENTATION OF THE SIMULATION FOR SINGLE IN-WHEEL MOTOR SYSTEM

In this subsection, we adopted Matlab/Simulink to implement simulations for a single in-wheel motor system. Table 2 shows the performance parameters of the in-wheel motor for simulation and the control flow chart of the motor under the SMO-NTSMC strategy is shown in Fig 5.

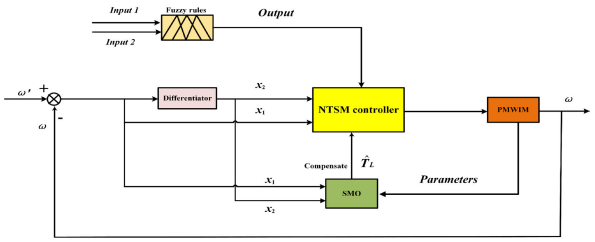

FIGURE 5. Control flow chart of the in-wheel system under the SMO-NTSMC strategy.

For the purpose of testing the starting performance, we give a starting speed instruction $(\omega' = 1200r/\min)$ to the PMIWM system and simulate the starting performance of the SMO-NTSMC scheme, NTSMC scheme, and conventional SMC scheme, the control parameters and control algorithm of NTSMC and conventional SMC scheme are referred to [41], [42], respectively. The starting performance simulations of these schemes are presented in Fig. 6. Fig. 7 shows the response performance of the control system when undergoing an external torque load of 20N·m at 1.0s. Fig. 8 illustrates the speed simulation of the motor system that receives a -20N·m unload instruction at 2.0s.

For the purpose of verifying the speed tracking capability of the SMO-NTSMC scheme, we implement simulations which receive two different time-varying speed instruction, Fig. 9 presents the speed simulation of the PMIWM system that receives a cosine function speed command $(\omega' = 1200 \cdot \cos(4\pi t))$ under the SMO-NTSMC strategy and NTSMC strategy respectively. Fig. 10 shows the track performance of these two strategies which receive a pin speed signal. Fig 11 and Fig 12 presents the output value of torque

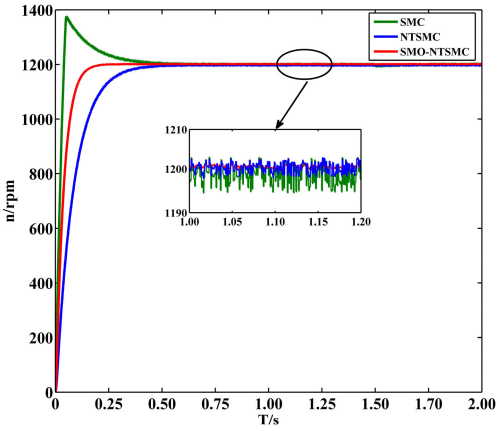

FIGURE 6. Starting response of single PMIWM of three control strategies.

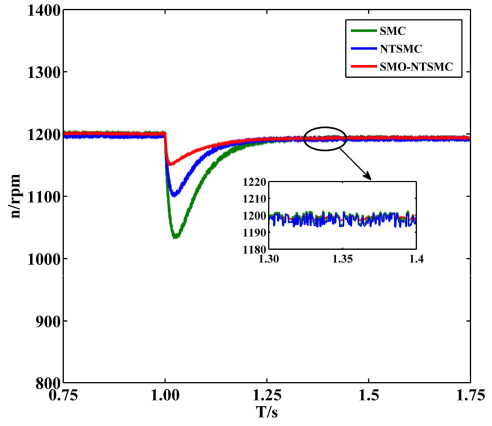

FIGURE 7. Speed curve of receiving load.

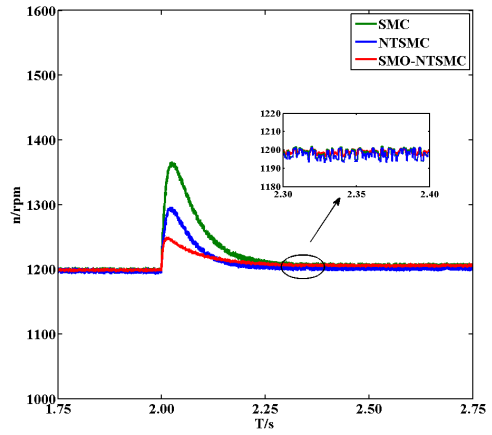

FIGURE 8. Speed curve of receiving unload.

and current when receiving step torque and linear step torque respectively to test the effectiveness of SMO.

Fig 6 presents the starting performance of the single PMIWM motor under the control strategies of SMO-NTSMC, NTSMC, and conventional SMC. It can be seen clearly that SMO-NTSMC and NTSMC strategies can respond to starting instruction without overshoot value, but the SMC scheme shows large overshoot value when the

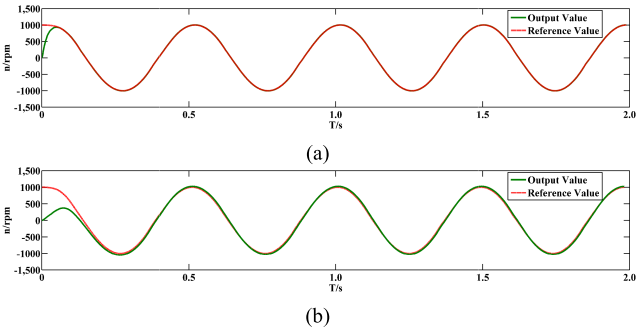

FIGURE 9. Speed track curve of the system (cosine signal) (a) SMO-NTSMC. (b) NTSMC.

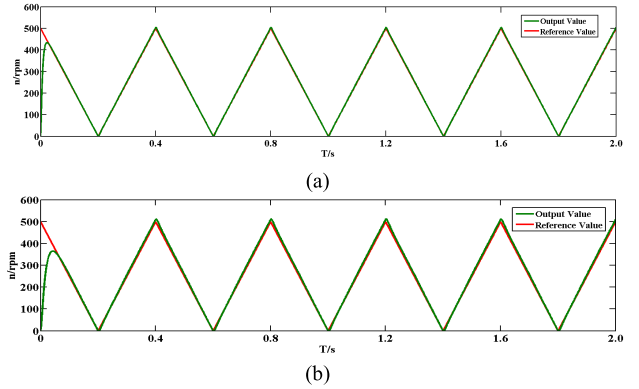

FIGURE 10. Speed track curve of the system (pin signal) (a) SMO-NTSMC. (b) NTSMC.

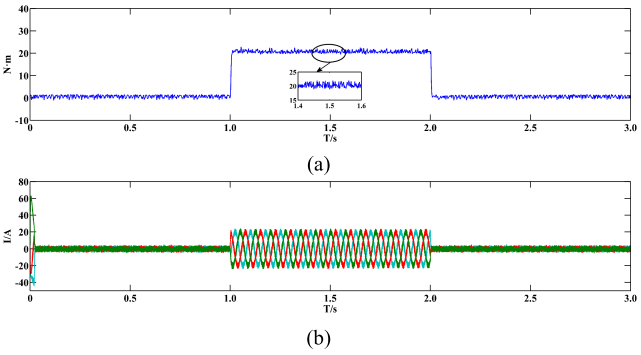

FIGURE 11. Output value of torque and current when receiving step torque (a) Torque value. (b) Current value.

control system starts up, and this overshoot phenomenon can seriously deteriorate the accuracy and performance of the control object. When it comes to the proposed SMO-NTSMC and NTSMC strategy, this simulation result shows that SMO-NTSMC consumes less response time than the NTSMC scheme when receives the starting instruction. In addition, from the 1.0-1.2 second magnification of Fig 6, we can observe that the proposed SMO-NTSMC scheme illustrates smaller speed fluctuation than NTSMC and SMC strategy when the steady-state is achieved

As shown in Fig 7 and Fig 8, speed simulations of the single PMIWM speed are presented when receives a load instruction at 1.0s and an unload instruction at 2.0s of the

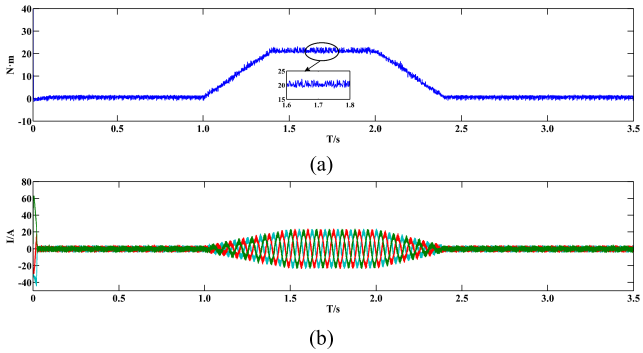

FIGURE 12. Output value of torque and current when receiving linear torque (a) Torque value. (b) Current value.

SMO-NTSMC, NTSMC, and SMC strategies. It is clear that the SMO-NTSMC scheme owns a quicker response speed than the other two strategies both with the load and unload instructions. Besides, the proposed SMO-NTSMC scheme presents less speed variation than the other two methods during the speed adjustment period. When the system returns to the steady-state, SMO-NTSMC shows smaller speed variation and owns better control performance than the others. The specific data comparison of the three control strategies is shown in Table 3.

Fig 9 and Fig 10 show tracking performances of the single PMIWM system when receiving speed instructions which change with time. It can be seen from these two simulations that the SMO-NTSMC consumes less time to track the reference value than the other scheme. In addition, we can observe that when the control object receives the variable speed instruction of cosine signal and pin signal, there are track errors exist in the control system when the control speed reaches the steady-state under the NTSMC strategy, while the SMO-NTSMC possess better track performance. The comparison of these two control strategies with the time-varying speed signal is shown in Table 4.

As shown in Fig 11(a), When the control system receives instructions of a 20N·m load at 1s and a −20N·m unload at 2s, the SMO of the proposed control strategy presents ideal torque estimation capability, and the torque error fluctuation is within 1.5N·m, which will not affect the safety and stability of the vehicle. In addition, we can observe from Fig 11(b) that the curve of three-phase current i_{adc} is stable and shows slight fluctuation in general.

Fig 12 shows the torque estimation of SMO and three-phase current i_{adc} of a single PMIWM system when receives a linear increasing torque in 1s and a linear decreasing torque at 2s. It is obvious that the proposed SMO of the system possesses excellent observe performance when receives a time-varying torque signal. Also, the three-phase current i_{adc} of PMIWM is relatively smooth.

From the above simulation of the single PMIWM system, we can obtain that the proposed SMO-NTSMC strategy has the following three merits through with other two strategies: 1) owns quicker starting and response speed. 2) has stronger

TABLE 1. Corresponding relation of fuzzy parameters.

$\phi(s)$ \ $\hat{h}(s\|\theta_h^*)$	NB	NM	ZO	PM	PB
NB	NB	NB	NM	NM	NM
NM	NB	NM	NM	ZO	ZO
ZO	NM	ZO	ZO	ZO	ZO
PM	NM	ZO	ZO	PM	PM
PB	PM	PM	PM	PB	PB

TABLE 2. Parameters of the PMIWM.

	SMO-NTSMC	NTSMC	SMC
Startup time (s)	0.142	0.474	0.515
Startup overshoot	0	0	24.3%
Adjust time(20N·m) (s)	0.193	0.212	0.304
Adjust time(-20N·m) (s)	0.188	0.221	0.298
Adjust fluctuate (20N·m) (percent)	4.93%	8.25%	15.61%
Adjust fluctuate (-20N·m) (percent)	4.88%	8.13%	16.42%

TABLE 3. comparison of the speed responses.

	SMO-NTSMC	NTSMC
Tracking time (s) (cosine signal)	0.142	0.474
Tracking time (s) (pin signal)	0.083	0.114
Steady error ((percent)) (cosine signal)	2.35%	5.32%
Steady error ((percent)) (pin signal)	4.29%	8.57%

TABLE 4. comparison of the tracking performance.

SYMBOL	QUANTITY	VALUE
B	Viscous friction coefficient	0.010N·m·s
Lq	Inductance of q axis	8.0mH
Ld	Inductance of d axis	8.0mH
J	Moment of inertia	0.008kg·m2
ψ	Rotor's magnetic flux	0.295Wb
R	Nominal phase resistance	2.385Ω
P_n	pole pairs	4
f	Switching frequency	8kHz
Q	Rated power	5kW

robustness and better dynamic performance. 3) owns better tracking ability when giving variable command.

B. IMPLEMENTATION OF THE SIMULATION FOR MULTI-MOTOR SYSTEM

For the purpose of verifying the effectiveness of the proposed ELS scheme for Multi-Motor system in this paper, we establish this system which combined with two front-drive motors in the DDEV system. Because the parameters of two-front drive motors cannot be exactly the same due to the internal structure and external disturbance, we denote Motor 2 with

TABLE 5. Parameters of the multi-motor system.

SYMBOL	Quantity	Motor 1	Motor 2
B	Viscous friction coefficient	0.008N·m·s	0.008+ ΔB N·m·s
Lq	Inductance of q axis	10.0mH	10.0mH
Ld	Inductance of d axis	10.0mH	10.0mH
J	Moment of inertia	0.004kg·m^2	0.004+ ΔJ kg·m^2
ψ	Rotor's magnetic flux	0.285Wb	0.285Wb
R	Nominal phase resistance	2.375Ω	2.375Ω
P_n	Number of pole pairs	4	4
f	Switching frequency	8kHz	8kHz
Q	Rated power	5kW	5kW

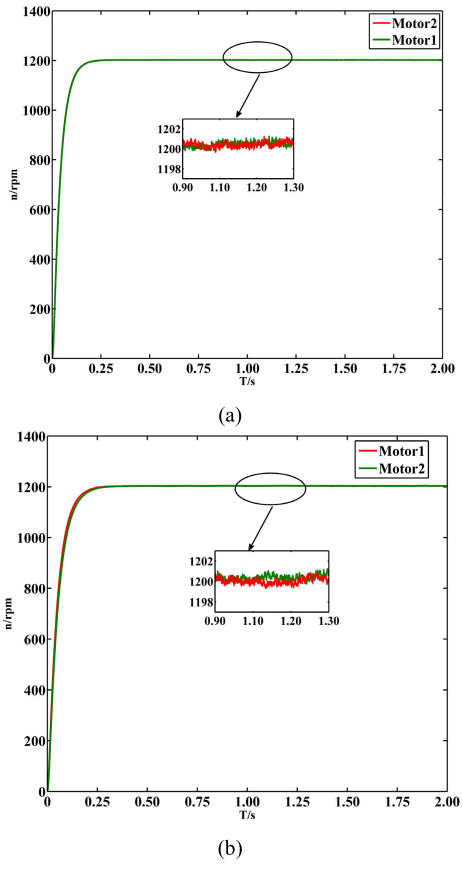

FIGURE 13. Starting tracking performance of Multi-Motor system (a)ELS. (b) Master-Slave.

parameters variation ($B + \Delta B$, $J + \Delta J$), and the parameters of motors are shown in Table 5. In the following simulations, we give instructions of starting, loading, and unloading to the Multi-Motor system and observe the tracking performance between two motors.

Fig 13 shows the starting performance of the Multi-Motor system under the strategies of the proposed ELS scheme and Master-Slave scheme and Fig 14 presents the tracking

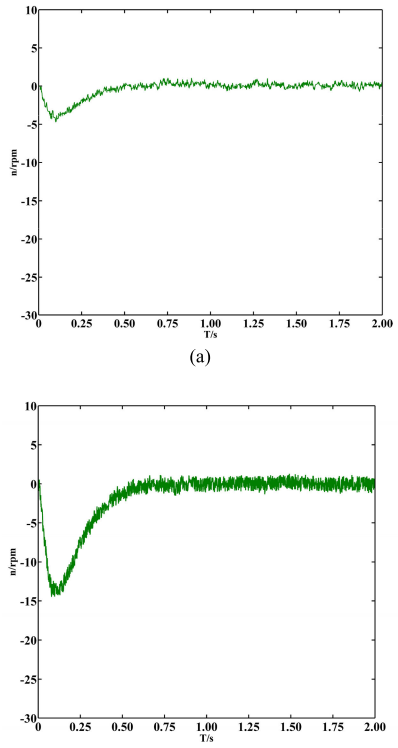

FIGURE 14. Starting tracking error of Multi-Motor system (a)ELS. (b) Master-Slave.

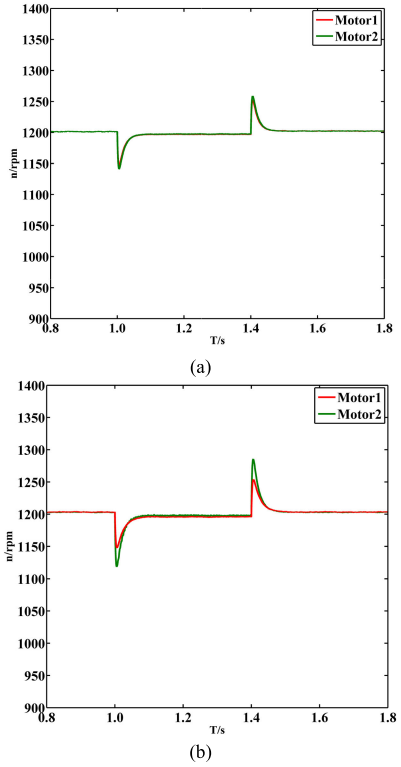

FIGURE 15. Load tracking performance of Multi-Motor system (a) ELS. (b) Master-Slave.

error of them. As shown in Fig 14 (a), the tracking error of two motors is under 5 r/min under the ELS control scheme, which presents ideal starting tracking performance. However,

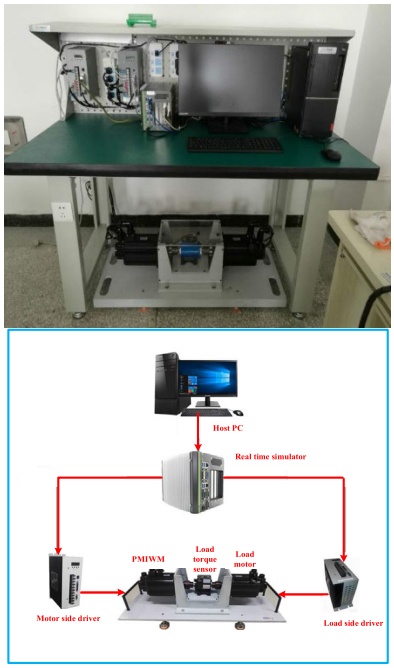

FIGURE 16. Experimental platform of the motor system.

the tracking error of the Master-Slave scheme is around 3 times the value of the ELS scheme. In addition, as shown in Fig 13 (a) and Fig 13 (b), we can observe from when the Multi-Motor reaches the steady-state, the proposed ELS scheme presents less tracking error than the Master-Slave scheme.

In order to simulate the road condition in which two front-drive of DDEV can undergo different load torque, we gave different load and unload to two motors in the Multi-Motor system and observe the speed tracking of them. For Motor 1, we gave it a 30 N·m external load in 1s and a −30N·m external unload at 1.4 s. For Motor 2, the external load and unload instructions of it are 15 N·m and −15N·m, and the simulations of Multi-Motor system with ELS and Master-Slave strategies are shown in Fig 15. We can observe from Fig 15 that the tracking error of two motors with the proposed ELS strategy is less than 20r/min when receiving different load and unload instructions, while the value of the Master-Slave strategy is more than 80 r/min, which is more than 4 times the error of ELS strategy.

From the simulation of the multi-motor control system, we can summarize that the proposed ELS strategy has the following advantages: 1) presents less starting tracking error of multi-motor system 2) owns better anti-jamming ability when the control system undergoes external disturbances. 3) presents less steady-error when the multi-motor system reaches the stable state.

C. EXPERIMENTS AND ANALYSIS

In order to further verify the simulation results of the control strategy proposed in this paper, the experimental platform

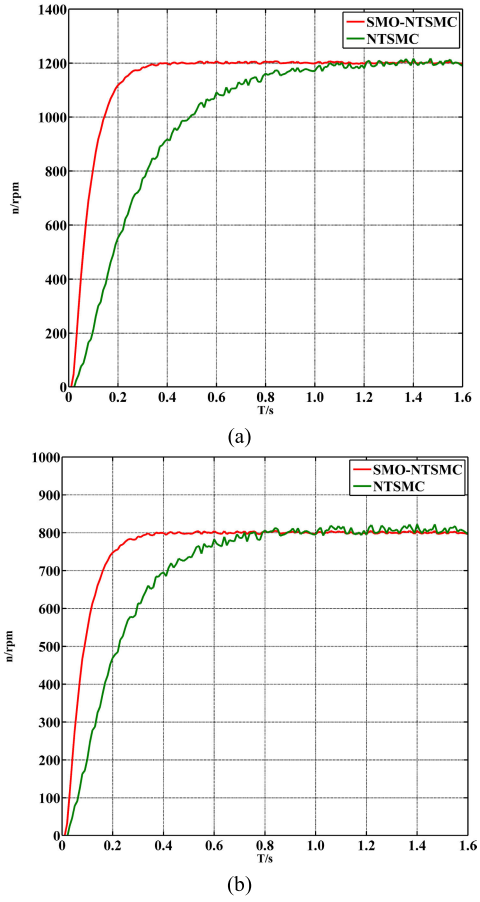

FIGURE 17. Experimental results of starting responses under the control strategies (a) 1200r/min (b) 800r/min.

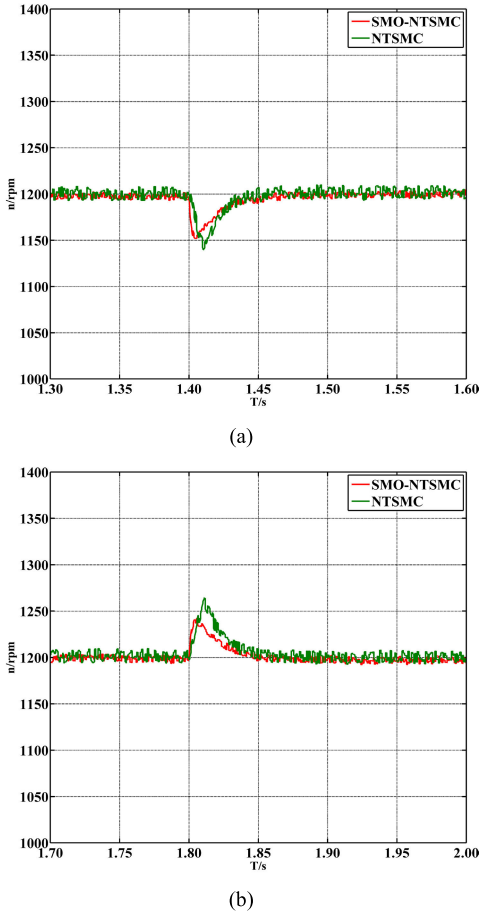

FIGURE 18. Experimental results of speed responses under the control strategies (1200r/min)(a) 30N·m (b) −30N·m.

of the motor system is built, and several experiments are implemented, which is shown in Fig 16. The executive module is combined with two PMIWMs, each one of them has a load motor to provide torque and a load torque sensor to observe torque. The control module mainly includes a host PC, Real-time simulator (made in China), load torque sensor (made in China), PMIWM (made in Japan), and load motor (made in China). Signal instructions such as motor speed and torque are sent by the host PC, then the Real-time simulator sends control signals to the motor side driver and load side driver which can drive PMIWM and load motor respectively.

In the first experiment, we take the single PMIWM control system as the experimental object. experimental results present the control performance and robustness of SMO-NTSMC strategy and NTSMC strategy respectively. Fig 17 (a)(b) compared the starting speed of these two strategies when receiving 800 r/min and 1200 r/min starting instruction. Fig 18 and Fig 19 presents the response performance of the PMIWM control system of SMO-NTSMC and NTSMC control scheme, which receive load and unload instructions under the speed of 1200r/min. Fig 20 and Fig 21 show the torque which tested the load torque sensor of PMIWM under the SMO-NTSMC and NTSMC control scheme respectively.

Fig 17 compares the starting performance of SMO-NTSMC and NTSMC scheme when receiving two starting instructions of 1200 r/min and 800 r/min respectively. As shown in this Figure, the proposed SMO-NTSMC scheme consumes less time to reach the stable state than the other scheme. In addition, when arriving at the command speed, the speed chattering of the SMO-NTSMC strategy is within 5 r/min, while that of NTSMC is more than 25 r/min. Therefore, the proposed SMO-NTSMC presents an ideal starting and steady performance.

Fig 18(a)(b) presents the response performance of the single-motor system when receiving a 20N·m load instruction at 1.4s and a −20N·m unload instruction at 1.8s. As shown in Fig 17(a), when giving the motor a load instruction under the speed of 1200r/min, both the proposed SMO-NTSMC and NTSMC scheme can return to steady speed no more than 0.08s, while the overshoot value of the NTSMC scheme is about 6.4%, which is almost twice that of SMO-NTSMC strategy.

Fig 19(a)(b) shows the speed response performance of the single-motor system when receiving the same load and

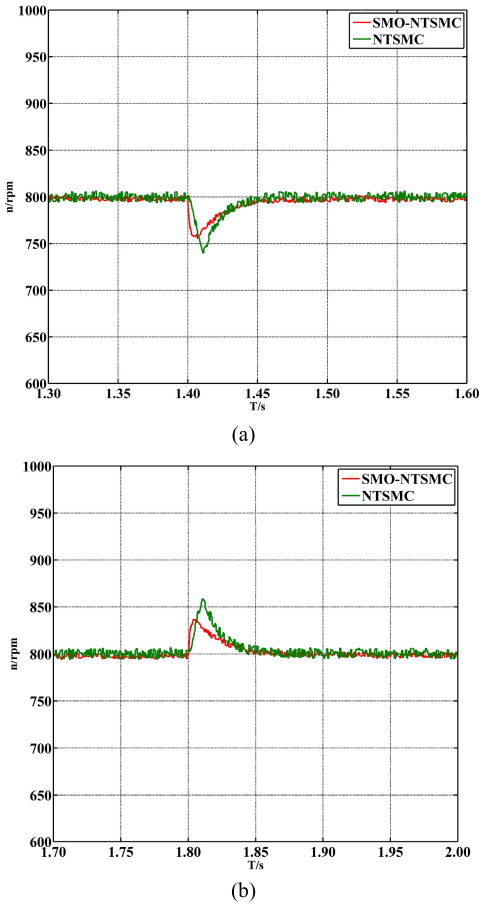

FIGURE 19. Experimental results of speed responses under the control strategies (800r/min)(a) 30N·m (b) −30N·m.

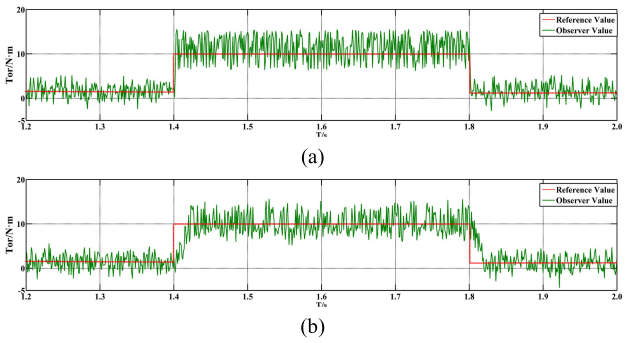

FIGURE 20. Experimental results of load torque observer when receiving torque command (10N·m) (a) BAS-NTSMC (b) NTSMC.

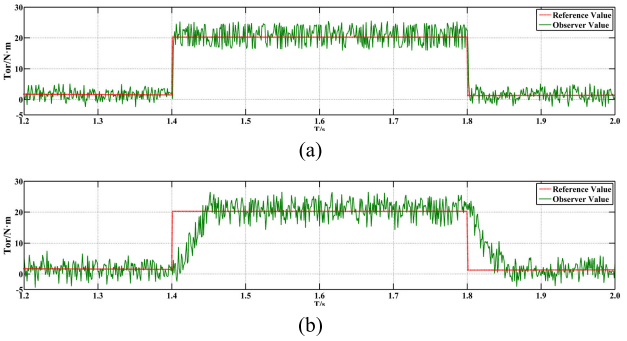

FIGURE 21. Experimental results of load torque observer when receiving torque command (20N·m) (a) BAS-NTSMC (b) NTSMC.

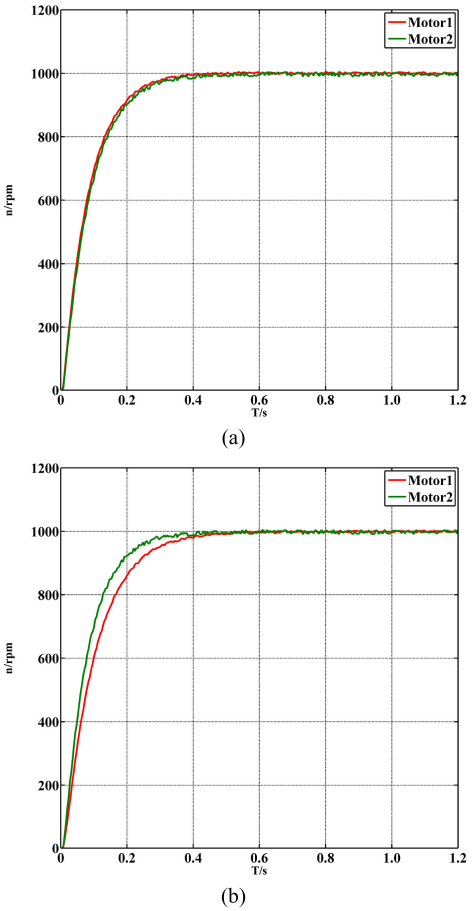

FIGURE 22. Experimental results of starting tracking performance of Multi-Motor system (1000 r/min) (a) ELS. (b) Master-Slave.

unload instructions under the speed of 800/min. The experimental results further verify the proposed strategy shows better anti-jamming ability and dynamic performance than the other.

Fig 20(a)(b) compares the torque value tested by the load torque sensors of the control object under the proposed SMO-NTSMC strategy and NTSMC strategy. As shown in Fig 20(a), when the PMIWM system receives a load instruction of 20N·m at 1.4s and an unload command of −20N·m at 1.8s, the adjust time of the proposed SMO-NTSMC scheme is about 0.1s, while that of the NTSMC strategy is 3 times of the proposed strategy. In addition, the overshoot of these two strategies is around 5 N·m, which is caused by the parameters and temperature variation of the control system.

As shown in 21(a)(b), when the PMIWM receives a load command of 10N·m at 1.4s and an unload command of −10N·m at 1.8s, the experimental result shows the proposed SMO-NTSMC scheme has a faster torque response with smaller overshoot than that of NTSMC strategy.

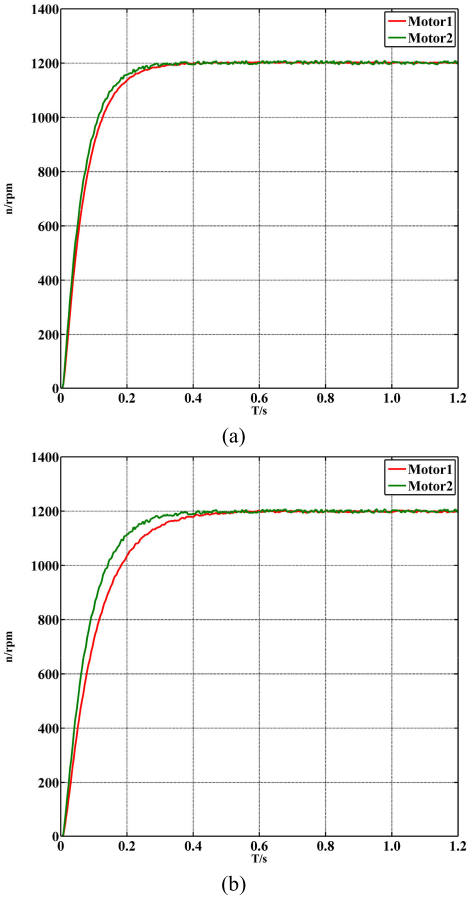

FIGURE 23. Experimental results of starting tracking performance of Multi-Motor system (1200 r/min) (a) ELS. (b) Master-Slave.

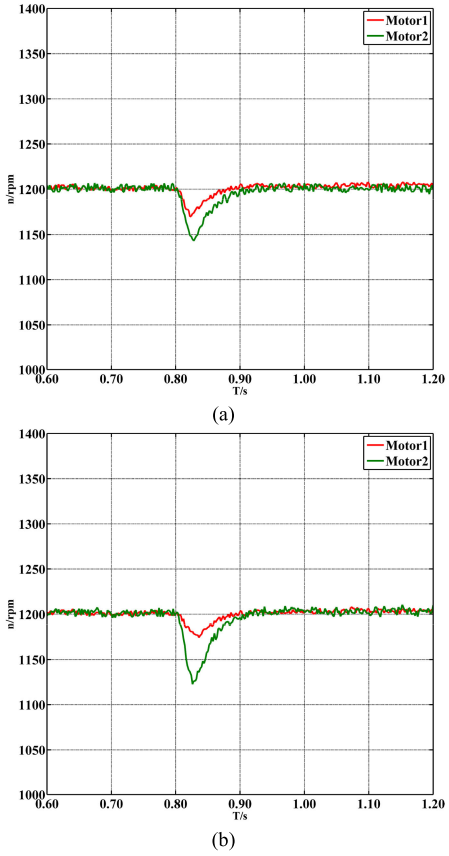

FIGURE 24. Experimental results of load tracking performance of Multi-Motor system (a)ELS. (b) Master-Slave.

In the second experiment, we take the Multi-Motor system as the experimental object to verify the anti-jamming ability and response speed of the proposed ELS scheme. Fig 22 and Fig 23 compared the starting speed of these two strategies when receiving 1000 r/min and 1200 r/min starting instruction. Fig 24 and Fig 25 presents the response performance of the PMIWM control system of the proposed ELS and Master-Slave control scheme, which receive load and unload instructions under different running speeds.

In order to further simulate the road state on which DDEV drive, we gave different load and unload instruction to two motors in the Multi-Motor system and observe the speed tracking of them. For Motor 1, we gave it a 10 N·m load torque in 0.8 s and a −10N·m unload torque at 1.6 s. For Motor 2, the load and unload torque instructions of it are 20 N·m and −20N·m, and the experimental results of the Multi-Motor system with ELS and Master-Slave strategies are shown in Fig 24 and Fig 25.

We can observe from Fig 24 and Fig 25 that the tracking error of two motors with the proposed ELS strategy is within 30 rpm when receives different load and unload instructions, while the value of the Master-Slave strategy is more than twice that of the proposed strategy.

As shown in Fig 22(a)(b), the experimental results show the starting tracking performance of the Multi-Motor system when receiving a 1000 r/min starting instruction. It is obvious that the proposed ELS control scheme presents less tracking error between two motors than the Master-Slave control scheme. The tracking error of two motors is within 10 r/min under the proposed ELS control scheme, while that of the Master-Slave scheme is more than 25 r/min.

Figure 23(a)(b) presents speed tracking experimental data when receiving a 1200 r/min starting instruction, in order to further verify the starting tracking performance of the proposed ELS control scheme. We can observe that the proposed strategy owns a better tracking performance than the Master-Slave strategy.

In summary, compared with other strategies, the proposed strategy:

1) has ideal starting performance and the anti-jamming ability for the single PMIWM system because of the proposed NTSMC strategy.
2) has smaller charting phenomenon during the control period because of the fuzzy algorithm to optimize the NTSMC parameters online.
3) Own the merits of better dynamic performance and robustness performance for single PMIWM through the load torque observer to observe the output torque in real-time

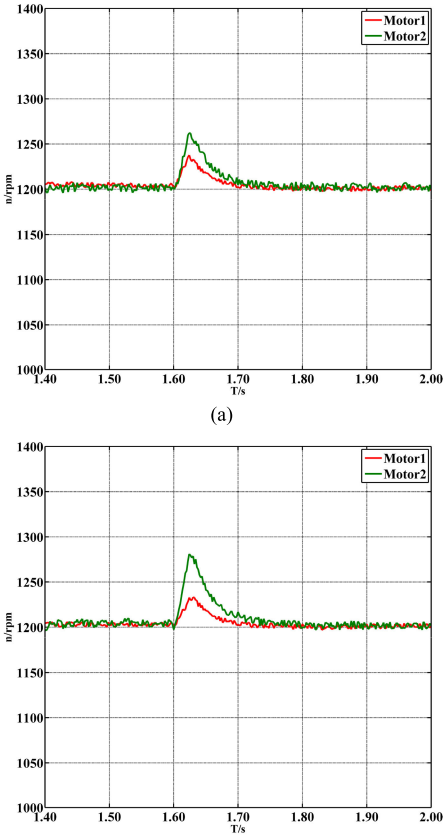

FIGURE 25. Experimental results of unloading tracking performance of Multi-Motor system (a)ELS. (b) Master-Slave.

4) For Multi-Motor system, has less tracking error between two motors during the starting and load period, verify that this control scheme can realize ideal synchronous control performance.

V. CONCLUSION

An SMO-NTSMC scheme Based on fuzzy rules is proposed in this paper to improve the dynamic performance and anti-jamming ability of the single motor system, and a novel ELS control scheme on the basis of the TACC algorithm is suggested to realize the synchronous control of each in-wheel motor installed on the DDEV. The following conclusions can be summarized from the simulation and experiments we have implemented.

1) Through adopting the NTSMC strategy combined with SMO, the response speed can be effectively accelerated with less time delay, and this method can effectively enhance the anti-jamming ability and the starting performance of the single-motor system.
2) By implementing the fuzzy algorithm to obtain the approaching parameter of NTSMC, the chattering value caused by the parameter variation has been eliminated.
3) A novel ELS control scheme on the basis of the TACC algorithm is suggested to realize the synchronous control of Multi-Motor system which can undergo different load torque on each motor, the experimental results

In conclusion, the proposed strategy can not only enhance the response speed and robustness of the single-motor system, but also realize ideal collaborative control of the Multi-Motor system. In addition, the chattering phenomenon can be effectively solved through the proposed fuzzy algorithm. Simulation and experimental results verify that the proposed method can be applied in the DDEV in the future.

In addition, the chattering phenomenon of the control system is still a trouble that cannot be completely reduced. In the future research, the fractional-order adaptive control will be adopted to further optimize the chattering phenomenon of the PMIWM system and the method proposed in this paper can adopted to other control system such as aircraft, robots, and hydraulic servo valves.

REFERENCES

[1] C. P. Lawrence, R. ElShatshat, M. M. A. Salama, and R. A. Fraser, "An efficient auxiliary system controller for fuel cell electric vehicle (FCEV)," *Energy*, vol. 116, pp. 417–428, Dec. 2016.
[2] X. Yuan, L. Li, H. Gou, and T. Dong, "Energy and environmental impact of battery electric vehicle range in China," *Appl. Energy*, vol. 157, pp. 75–84, Nov. 2015.
[3] L. Zhang, W. Liu, and B. Qi, "Innovation design and optimization management of a new drive system for plug-in hybrid electric vehicles," *Energy*, vol. 186, Nov. 2019, Art. no. 115823.
[4] L. P. Zhang, W. Liu, and B. Qi, "Optimization of multi-mode coupling drive plug-in hybrid electric vehicles based on speed prediction Energy," *Energy*, vol. 206, pp. 118–126, Sep. 2020.
[5] X. Zhang, D. Gohlich, and J. Li, "Energy-efficient toque allocation design of traction and regenerative braking for distributed drive electric vehicles," *IEEE Trans. Veh. Technol.*, vol. 67, no. 1, pp. 285–295, Jan. 2018.
[6] L. Zhai, T. Sun, and J. Wang, "Electronic stability control based on motor driving and braking torque distribution for a four in-wheel motor drive electric vehicle," *IEEE Trans. Veh. Technol.*, vol. 65, no. 6, pp. 4726–4739, Jun. 2016.
[7] G. Wang, X.-L. Liu, C. Lin, and K.-S. Zhang, "The research of traction control for the distributed driven electric vehicle," in *Proc. IEEE Conf. Expo Transp. Electrific. Asia–Pacific (ITEC Asia–Pacific)*, Beijing, China, Aug. 2014, pp. 1–4, doi: 10.1109/ITEC-AP.2014.6941092.
[8] H. Peng, W. Wang, C. Xiang, L. Li, and X. Wang, "Torque coordinated control of four in-wheel motor independent-drive vehicles with consideration of the safety and economy," *IEEE Trans. Veh. Technol.*, vol. 68, no. 10, pp. 9604–9618, Oct. 2019.
[9] T. Lubin, S. Mezani, and A. Rezzoug, "Two-dimensional analytical calculation of magnetic field and electromagnetic torque for surface-inset permanent-magnet motors," *IEEE Trans. Magn.*, vol. 48, no. 6, pp. 2080–2091, Jun. 2012.
[10] B. Leng, L. Xiong, Z. Yu, K. Sun, and M. Liu, "Robust variable structure anti-slip control method of a distributed drive electric vehicle," *IEEE Access*, vol. 8, pp. 162196–162208, Sep. 2020.
[11] C. Zhang, J. Hu, J. Qiu, W. Yang, H. Sun, and Q. Chen, "A novel fuzzy observer-based steering control approach for path tracking in autonomous vehicles," *IEEE Trans. Fuzzy Syst.*, vol. 27, no. 2, pp. 278–290, Feb. 2019.
[12] Z. Jingbo, C. Jie, and L. Chengye, "Stability coordinated control of distributed drive electric vehicle based on condition switching," *Math. Problems Eng.*, vol. 2020, pp. 1–10, Oct. 2020.
[13] J. Wang, Z. Luo, Y. Wang, B. Yang, and F. Assadian, "Coordination control of differential drive assist steering and vehicle stability control for four-wheel-independent-drive EV," *IEEE Trans. Veh. Technol.*, vol. 67, no. 12, pp. 11453–11467, Dec. 2018.
[14] G. Park, K. Han, K. Nam, H. Kim, and S. B. Choi, "Torque vectoring algorithm of electronic-four-wheel drive vehicles for enhancement of cornering performance," *IEEE Trans. Veh. Technol.*, vol. 69, no. 4, pp. 3668–3679, Apr. 2020.

[15] H. Huang, Q. Tu, M. Pan, C. Jiang, and J. Xue, "Fast terminal sliding mode control of permanent magnet in-wheel motor based on a fuzzy controller," *Energies*, vol. 13, pp. 188–216, Jan. 2020.

[16] X. Zhang and Z. Li, "Sliding-mode observer-based mechanical parameter estimation for permanent magnet synchronous motor," *IEEE Trans. Power Electron.*, vol. 31, no. 8, pp. 5732–5745, Aug. 2016.

[17] M. Wang, X. Dong, X. Ren, and Q. Chen, "SDRE based optimal finite-time tracking control of a multi-motor driving system," *Int. J. Control*, vol. 4, pp. 1–23, Jan. 2020.

[18] F.-K. Wu, T.-J. Yeh, and C.-F. Huang, "Motor control and torque coordination of an electric vehicle actuated by two in-wheel motors," *Mechatronics*, vol. 23, no. 1, pp. 46–60, Feb. 2013.

[19] C. Yu, X. Wang, X. Xu, M. Zhang, H. Ge, J. Ren, L. Sun, B. Chen, and G. Tan, "Distributed multiagent coordinated learning for autonomous driving in highways based on dynamic coordination graphs," *IEEE Trans. Intell. Transp. Syst.*, vol. 21, no. 2, pp. 735–748, Feb. 2020.

[20] X. Shi, J. Cao, and W. Huang, "Distributed parametric consensus optimization with an application to model predictive consensus problem," *IEEE Trans. Cybern.*, vol. 48, no. 7, pp. 2024–2035, Jul. 2018.

[21] T. Zhang, Y. Zou, X. Zhang, N. Guo, and W. Wang, "Data-driven based cruise control of connected and automated vehicles under cyber-physical system framework," *IEEE Trans. Intell. Transp. Syst.*, vol. 48, no. 7, pp. 2024–2035, Jul. 2018.

[22] C. Lin, S. Liang, J. Chen, and X. Gao, "A multi-objective optimal torque distribution strategy for four in-wheel-motor drive electric vehicles," *IEEE Access*, vol. 7, pp. 64627–64640, May 2019.

[23] W. Li, X. Zhu, and J. Ju, "Hierarchical braking torque control of in-wheel-motor-driven electric vehicles over CAN," *IEEE Access*, vol. 6, pp. 65189–65198, Oct. 2018.

[24] D. Tan, H. Xue, K. Yang, A. Li, and H. Wang, "Study on the thermal characteristics of in-wheel motor drive system based on driving cycles," *IEEE Access*, vol. 7, pp. 14463–14471, Dec. 2019.

[25] J. Kim, C. Park, S. Hwang, Y. Hori, and H. Kim, "Control algorithm for an independent motor-drive vehicle," *IEEE Trans. Veh. Technol.*, vol. 59, no. 7, pp. 3213–3222, Sep. 2010.

[26] B. Jandaghi and V. Dinavahi, "Hardware-in-the-Loop emulation of linear induction motor drive for MagLev application," *IEEE Trans. Plasma Sci.*, vol. 44, no. 4, pp. 679–686, Apr. 2016.

[27] P. Zheng, Y. Sui, J. Zhao, C. Tong, T. A. Lipo, and A. Wang, "Investigation of a novel five-phase modular permanent-magnet in-wheel motor," *IEEE Trans. Magn.*, vol. 47, no. 10, pp. 4084–4087, Oct. 2011.

[28] R. Ma and G. Zhang, "Sliding mode tracking control with differential evolution optimisation algorithm using integral-chain differentiator in uncertain nonlinear systems," *Int. J. Syst. Sci.*, vol. 49, no. 6, pp. 1345–1352, Mar. 2018.

[29] D. Terazono, J. Liu, Y. Miura, S. Sakabe, H. Bevrani, and T. Ise, "Grid frequency regulation support from back-to-back motor drive system with virtual-synchronous-generator-based coordinated control," *IEEE Trans. Power Electron.*, vol. 36, no. 3, pp. 2901–2913, Mar. 2021.

[30] V. Repecho, D. Biel, and A. Arias, "Fixed switching period discrete-time sliding mode current control of a PMSM," *IEEE Trans. Ind. Electron.*, vol. 65, no. 3, pp. 2039–2048, Mar. 2018, doi: 10.1109/TIE.2017.2745469.

[31] S. Li, M. Zhou, and X. Yu, "Design and implementation of terminal sliding mode control method for PMSM speed regulation system," *IEEE Trans. Ind. Informat.*, vol. 9, no. 4, pp. 1879–1891, Nov. 2013.

[32] A. Argha, S. W. Su, A. Savkin, and B. Celler, "Design of optimal sliding-mode control using partial eigenstructure assignment," *Int. J. Control*, vol. 92, no. 7, pp. 1511–1523, Nov. 2017.

[33] S. Song, B. Zhang, J. Xia, and Z. Zhang, "Adaptive backstepping hybrid fuzzy sliding mode control for uncertain fractional-order nonlinear systems based on finite-time scheme," *IEEE Trans. Syst., Man, Cybern. Syst.*, vol. 50, no. 4, pp. 1559–1569, Apr. 2020.

[34] S. Song, B. Zhang, X. Song, Y. Zhang, Z. Zhang, and W. Li, "Fractional-order adaptive neuro-fuzzy sliding mode H_∞ control for fuzzy singularly perturbed systems," *J. Franklin Inst.*, vol. 356, no. 10, pp. 5027–5048, Jul. 2019.

[35] K.-K. Shyu, Y.-W. Tsai, and C.-K. Lai, "Sliding mode control for mismatched uncertain systems," *Electron. Lett.*, vol. 34, no. 24, pp. 2359–2360, Nov. 1998.

[36] J. Wang, L. Zhao, and L. Yu, "Adaptive terminal sliding mode control for magnetic levitation systems with enhanced disturbance compensation," *IEEE Trans. Ind. Electron.*, vol. 68, no. 1, pp. 756–766, Jan. 2021.

[37] Y. Xue, B.-C. Zheng, and X. Yu, "Robust sliding mode control for T-S fuzzy systems via quantized state feedback," *IEEE Trans. Fuzzy Syst.*, vol. 26, no. 4, pp. 2261–2272, Aug. 2018.

[38] H. Pan and W. Sun, "Nonlinear output feedback finite-time control for vehicle active suspension systems," *IEEE Trans. Ind. Informat.*, vol. 15, no. 4, pp. 2073–2082, Apr. 2019.

[39] H. Pan, W. Sun, H. Gao, and X. Jing, "Disturbance observer-based adaptive tracking control with actuator saturation and its application," *IEEE Trans. Autom. Sci. Eng.*, vol. 13, no. 2, pp. 868–875, Apr. 2016.

[40] X. Yu, Y. Fu, P. Li, and Y. Zhang, "Fault-tolerant aircraft control based on self-constructing fuzzy neural networks and multivariable SMC under actuator faults," *IEEE Trans. Fuzzy Syst.*, vol. 26, no. 4, pp. 2324–2335, Aug. 2018.

[41] X. Zhang and Y. He, "Direct voltage-selection based model predictive direct speed control for PMSM drives without weighting factor," *IEEE Trans. Power Electron.*, vol. 34, no. 8, pp. 7838–7851, Aug. 2019.

[42] Y. Jiang, W. Xu, C. Mu, and Y. Liu, "Improved deadbeat predictive current control combined sliding mode strategy for PMSM drive system," *IEEE Trans. Veh. Technol.*, vol. 67, no. 1, pp. 251–263, Jan. 2018.

HAO HUANG was born in Hunan, China, in 1995. He received the B.S. degree in mechanical engineering and automation from Wuhan University, China, in 2016, and the M.S. degree in mechanical engineering from the Army Engineering University of PLA, China, in 2018, where he is currently pursuing the Ph.D. degree in mechanical engineering. His research interests include electric machines and drives, and intelligent control.

QUNZHANG TU was born in Hubei, China, in 1969. He received the B.S. and M.S. degrees in mechanical design and theory from the Engineering Institute of the Engineer Corps, China, in 1987 and 1995, respectively, and the Ph.D. degree in mechanical design and theory from the PLA University of Science and Technology, in 2001. He is currently a Professor with the Army Engineering University of PLA. His research interests include mechanical and electrical control and transmission, and mechatronics.

CHENGMING JIANG was born in Jiangsu, China, in 1973. He received the B.S. degree from Southeast University, China, in 2001, and the M.S. degree in computer application technology from Jiangsu University, China, in 2007. He is currently an Associate Professor with the Army Engineering University of PLA. His research interests include electrical control and transmission, and motor control.

MING PAN was born in Jilin, China, in 1987. He received the B.S. degree in mechanical engineering and automation from Tsinghua University, in 2016, and the M.S. and Ph.D. degrees in military equipment from the Army Engineering University of PLA, in 2012 and 2016 respectively. He is currently a Lecturer with the Army Engineering University of PLA. His research interests include hybrid vehicles and general control technique.

CHANGLIN ZHU was born in Shaanxi, China, in 1997. He received the B.S. degree in mechanical engineering and automation from the Field Engineering College, Army Engineering University of PLA, China, in 2019, where he is currently pursuing the M.S. degree. His research interests include electric machines and drives, and intelligent control.